arXiv:1701.04567v1 [physics.flu-dyn] 17 Jan 2017

The effect of turbulence on mass and heat transfer rates of small inertial particles

Nils Erland L. Haugen[1,2], Jonas Krüger[1], Dhrubaditya Mitra[3] and Terese Løvås[1]

[1]Department of Energy and Process Engineering, Norwegian University of Science and Technology, Kolbjørn Hejes vei 1B, NO-7491 Trondheim, Norway
[2]SINTEF Energy Research, N-7465 Trondheim, Norway
[3]Nordita, KTH Royal Institute of Technology and Stockholm University, Roslagstullsbacken 23, SE-10691 Stockholm, Sweden

(Received)

The effect of turbulence on the mass and heat transfer between small heavy inertial particles (HIP) and an embedding fluid is studied. Two effects are identified. The first effect is due to the relative velocity between the fluid and the particles, and a model for the relative velocity is presented. The second effect is due to the clustering of particles, where the mass transfer rate is inhibited due to the rapid depletion of the consumed species inside the dense particle clusters. This last effect is relevant for large Damköhler numbers and it may totally control the mass transfer rate for Damköhler numbers larger than unity. A model that describes how this effect should be incorporated into existing particle simulation tools is presented.

Key words: Reacting multiphase flow, Particle/fluid flow, Combustion, Turbulent reacting flows, Turbulence simulations

1. Introduction

Both in nature and in industrial applications, one regularly finds small inertial particles embedded in turbulent flows. By small inertial particles, we mean particles that are smaller than the smallest scales of the turbulence and have significantly higher material density than the fluid. For such particles, there will be momentum exchange between the particles and the turbulent fluid, and, depending on the conditions, there may also be heat and mass transfer. This is particularly so for chemically reacting particles, but there are also a large number of other applications where heat and mass transfer between particles and fluid are important. Here, the main focus will be on reacting particles that consume one or more of the species in the embedding gas through surface reactions. Relevant examples are; chemical reactions on the surface of a catalytic particle, fuel oxidation on the surface of a oxygen carrying particle in a Chemical Looping Combustion (CLC) reactor, condensation of water vapor on cloud droplets and combustion or gasification of char.

The presence of turbulence in a fluid will enhance the transport properties of the flow. This means that the mean-field viscosity, diffusivity and conductivity may be drastically increased from their laminar values. This effect has been studied for many years, and a large number of different models exist in the literature, such as the k-ϵ model (Jones & Launder (1972)) and different versions of the Reynolds Stress Models (e.g. Pope (2003)). Turbulence may also modify gas phase combustion, and even though this is somewhat more complicated, a significant number of models have been developed during the last decades. Some examples are the Eddy Dissipation Model (Magnussen & Hjertager (1976)), the Eddy Dissipation Concept (Ertesvåg & Magnussen (2000)) and variations of Probability Density Function (e.g. Dopazo (1994)) models.

With the above knowledge in mind, it is interesting to realize that, except for the recent work

of Kruger et al. (2016), there is currently no model describing the effect of turbulence on the heat and mass transfer of small inertial particles. When a reacting particle is embedded in a turbulent flow, the turbulence can potentially influence the mass transfer, and hence the surface reaction rates in two ways. The first way is through particle clustering, where particles form dense clusters due to turbulence, and where the gas phase reactants within the cluster are quickly consumed while there are no particles that can consume the reactants in the particle voids outside the clusters. The main effect of the clustering is to *decrease* the overall mass transfer rate. The second way turbulence influence the mass transfer rate is by increasing the mean velocity difference between the particle and the gas. This effect will *increase* the mass transfer rate.

The same two effects are also active for the heat transfer. The similarity between heat and mass transfer can be seen by considering the expressions for the transfer coefficients of mass

$$\kappa = \frac{\mathrm{Sh}D}{d_p} \tag{1.1}$$

and heat

$$\kappa_{\mathrm{th}} = \frac{\mathrm{Nu}D_{\mathrm{th}}}{d_p}, \tag{1.2}$$

where d_p is the particle radius, Sh and Nu are the Sherwood and Nusselt numbers and D and D_{th} are the mass and thermal diffusivities. For single spherical particles in flows with low and medium particle Reynolds numbers, the Sherwood and Nusselt numbers can be approximated by the empirical expressions of Ranz & Marshall (1952)

$$\begin{aligned} \mathrm{Sh}_{\mathrm{RM}} &= 2 + 0.69\mathrm{Re}_p^{1/2}\mathrm{Sc}^{1/3} \\ \mathrm{Nu}_{\mathrm{RM}} &= 2 + 0.69\mathrm{Re}_p^{1/2}\,\mathrm{Pr}^{1/3}. \end{aligned} \tag{1.3}$$

A well known example where reacting particles are consumed in a turbulent fluid is the case of pulverized coal combustion, where turbulence influences the process in several ways that are understood to varying degrees. The combustion of coal can be divided into four separate processes; 1) drying, 2) devolatilization, 3) combustion of volatiles and 4) burnout of the remaining char. Processes 1 and 2 involve the evaporation of fluids and thermal cracking of hydrocarbons, while process 3 involves homogeneous reactions. In process 4, gas phase species diffuse to the particle surface and react with the solid carbon. This happens via adsorption of e.g. an oxygen radical to a carbon site on the particle surface and a subsequent desorption of carbon monoxide into the gas phase. This makes process 4 dominated by heterogeneous chemical reactions. Many published studies utilize RANS based simulation tools that describe simulations of pulverized coal conversion in the form of combustion or gasification with an Eulerian-Eulerian approach (Gao et al. (2004) and Zhang et al. (2005)) or a Lagrangian-Eulerian approach (Silaen & Wang (2010); Vascellari et al. (2014, 2015); Klimanek et al. (2015); Chen et al. (2012, 2000)). However, none of these papers take the effect of turbulence on the heterogeneous char reactions into account. To the knowledge of the authors, the only studies where account is made for this effect are the papers of Luo et al. (2012); Brosh & Chakraborty (2014); Brosh et al. (2015) and Hara et al. (2015) where the Direct Numerical Simulations (DNS) approach is used. In a DNS, all turbulence scales are explicitly resolved on the computational grid, such that the effect of turbulence is implicitly accounted for. However, the DNS approach is extremely costly and can therefore only be used for small simulation domains. For simulations of large scale applications, the RANS or LES based simulation tools will therefore be the only applicable tools for the foreseeable future.

In the current paper, the same framework as was developed by Kruger et al. (2016) has been used and extended. The aim of the paper is to identify the effect of turbulence on the mass and

heat transfer of solid particles, and to develop models that describe this effect for all Damköhler numbers.

2. Mathematical model and implementation

In the current work, the so called point-particle direct numerical simulation (PP-DNS) approach is used. Here, the turbulent fluid itself is solved with the direct numerical simulation (DNS) methodology, where all turbulent scales are resolved and no modelling is needed. The particles are however not resolved, but rather treated as point particles where the fluid-particle momentum, mass and heat interactions are modelled. The point particle approach is a simplification that relies heavily on the quality of the models. The alternative approach, which is to resolve the particles and their boundary layer, is extremely CPU intensive and can currently not be done for more than a few hundred particles, even on the largest computers (Deen & Kuipers (2014)).

A number of simplifications are made in this paper. This has been done in order to make the simulations less CPU intensive, and, even more importantly, to isolate the dominating physical mechanisms. The particles are considered to be ever lasting, i.e. they are not consumed. The reaction on the particle surface is converting reactant A to product B;

$$A \rightarrow B \tag{2.1}$$

isothermally, i.e.; there is no production or consumption of heat, such that only the mass transfer effect is considered. As explained above, the effect on the heat transfer rate will be similar to the effect on the mass transfer rate. As reactant A is converted product B, the thermodynamical and transport properties are not changed.

2.1. *Fluid equations*

The equations determining the motion of the carrier fluid is give by the continuity equation

$$\frac{\partial \rho}{\partial t} + \nabla \cdot (\rho \boldsymbol{u}) = 0, \tag{2.2}$$

and the Navier–Stokes equation

$$\rho \frac{\mathrm{D}\boldsymbol{u}}{\mathrm{D}t} = -\boldsymbol{\nabla} P + \boldsymbol{\nabla} \cdot (2\mu \boldsymbol{S}) + \rho \boldsymbol{f} + \boldsymbol{F}. \tag{2.3}$$

Here, ρ, $\boldsymbol{u}$, $\mu = \rho\nu$ and ν are the density, velocity and dynamic and kinematic viscosities of the carrier fluid, respectively. The pressure P and the density ρ are related by the isothermal sound speed c_s, i.e.,

$$P = c_\mathrm{s}^2 \rho, \tag{2.4}$$

while the trace-less rate of strain tensor is given by

$$\boldsymbol{S} = \frac{1}{2}\left(\boldsymbol{\nabla u} + (\boldsymbol{\nabla u})^T\right) - \frac{1}{3}\boldsymbol{\nabla} \cdot \boldsymbol{u}. \tag{2.5}$$

Kinetic energy is injected into the simulation box through the forcing function f, which is solenoidal and non-helical and injects energy and momentum perpendicular to a random wave vector whose direction changes every time-step (Haugen et al. 2012; Kruger et al. 2016). Similar kinds of forcing has also previously been used for particle laden flows by other groups (Bec et al. 2007). The energy injection rate is maintained at a level such that the maximum Mach number is always below 0.5. The domain is cubic with periodic boundaries in all directions. The momentum exchange term, $\boldsymbol{F}$, is chosen to conserve momentum between the fluid and the solid particles, i.e.,

$$\boldsymbol{F} = -\frac{1}{V_\mathrm{cell}} \sum_\mathrm{k} m^k \boldsymbol{a}^k \tag{2.6}$$

when V_{cell} is the volume of the grid cell of interest and m^k and $\boldsymbol{a}^k$ are the mass and acceleration (due to fluid drag) of the k'th particle within the grid cell.

The equation of motion of the reactant has the well-known advection-reaction-diffusion form:

$$\frac{\partial X}{\partial t} + \nabla \cdot (X\boldsymbol{u}) = D\bar{M}_{\text{c}}\nabla \cdot (\nabla X) + \tilde{R}, \tag{2.7}$$

where X, $\bar{M}_{\text{c}}$ and D are the mole fraction, the mean molar mass and the diffusivity of the reactant, respectively. The last term in Eq. (2.7), $\tilde{R}$, is the sink term due to the gas-solid reactions on the surface of the solid particles.

2.2. *Particle equations*

The N_p particles that are embedded in the flow are treated as point particles, which means that they are assumed to be significantly smaller than the viscous scale of the fluid and the diffusive scale of the reactant. The motion of the k'th particle is described by the equations for position

$$\frac{d\boldsymbol{X}^{\text{k}}}{dt} = \boldsymbol{V}^{\text{k}} \tag{2.8}$$

and velocity

$$\frac{d\boldsymbol{V}^{\text{k}}}{dt} = \boldsymbol{a}^k \tag{2.9}$$

when the particle acceleration due to fluid drag is given by $\boldsymbol{a}^k = \frac{1}{\tau}\left[\boldsymbol{u}(\boldsymbol{X}^{\text{k}}) - \boldsymbol{V}^{\text{k}}\right]$. Note that gravity is neglected in this work. The particle response time is given by (Schiller & Naumann (1933))

$$\tau = \frac{\tau_{\text{St}}}{1 + f_c} \tag{2.10}$$

when $\tau_{\text{St}} = S\,d_p^2/18\nu$ is the Stokes time, $f_c = 0.15\text{Re}_p^{0.687}$ is a Reynolds number correction term to the classical Stokes time, $S = \rho_p/\rho$ is the density ratio, ρ_p is the material density of the particles,

$$\text{Re}_p = \frac{|\boldsymbol{u}(\boldsymbol{X}^{\text{k}}) - \boldsymbol{V}^{\text{k}}|d_p}{\nu} = \frac{u_{\text{rel}}d_p}{\nu} \tag{2.11}$$

is the particle Reynolds number and d_p is the particle diameter.

2.3. *Surface reactions*

Let us now model the reactive term. We assume that the reactions are limited to the surface of the particles and that the reactions are diffusion controlled, i.e. that all reactant that reaches the particle surface is consumed immediately†. The reactive term can then be written as

$$\tilde{R} = \frac{1}{V_{\text{cell}}}\sum_{\text{k}} A_p^k \kappa X_\infty^K \tag{2.12}$$

where $A_p = 4\pi r_p^2$ is the external surface area of the particle, the mass transfer coefficient is given by

$$\kappa = \frac{D\text{Sh}}{d_p} \tag{2.13}$$

and Sh is the Sherwood number.

To couple the reactive particle with the continuum equations we use the following prescription; for the k-th particle, which is at position $\boldsymbol{X}^{\text{k}}$, we set

$$X_\infty^k = X(\boldsymbol{X}^{\text{k}}), \tag{2.14}$$

† It is possible to relax the assumption of diffusion controlled reactions by also accounting for chemical kinetics at the particle surface, see Kruger et al. (2016).

i.e.; the far field reactant mole fraction is set equal to the reactant mole fraction of the fluid cell where the particle is. In the current work, the particle Sherwood number is determined by the expression of Ranz & Marshall (1952) (see Eq. (1.3) in the introduction), which is in contrast to the work of Kruger et al. (2016) where the Sherwood number was set to a constant value of 2, which corresponds to the Sherwood number in a quiescent flow. The particle Reynolds number is given by Eq. (2.11) and the Schmidt number, $\mathrm{Sc} = \nu/D$, is the ratio of the fluid viscosity and the mass diffusivity.

2.4. *The reactant consumption rate*

It is useful to define a reactant consumption rate as

$$\alpha = -\overline{\left(\frac{\tilde{R}}{X_\infty}\right)} = \overline{n_p A_p \kappa}, \tag{2.15}$$

when $\overline{O}$ represents the volume average of flow property O and n_p is the particle number density. If everything is assumed to be homogeneously distributed over the volume, the reactant consumption rate is given by

$$\alpha_{\mathrm{hom}} = n_p A_p \kappa = n_p A_p \frac{\mathrm{Sh} D}{d_p} \tag{2.16}$$

for a given particle size and number density.

In many RANS based simulation tools, where the local fluid velocity is not resolved, it is common to neglect the relative velocity difference between the turbulent eddies and the particles. This implies that $\mathrm{Sh} = 2$. Since the effect of particle clustering is also neglected in such models, the modelled reactant consumption rate becomes;

$$\alpha_{\mathrm{Sh,Da}} = \lim_{\mathrm{Sh}\to 2, \mathrm{Da}\to 0} \alpha = n_p A_p \frac{2D}{d_p}. \tag{2.17}$$

In the following, $\alpha_{\mathrm{Sh,Da}}$ will be used for normalization.

It is useful to define the Damköhler number, which is the ratio of the typical turbulent and chemical time scales, as

$$\mathrm{Da} = \frac{\tau_L}{\tau_c} \tag{2.18}$$

where $\tau_L = L/u_{\mathrm{rms}}$ is the integral time scale of the turbulence, L is the turbulent forcing scale, u_{rms} is the root-mean-square turbulent velocity and the chemical time scale is

$$\tau_c = 1/\alpha_{\mathrm{Sh,Da}}. \tag{2.19}$$

Particles in a turbulent flow field will tend to form clusters with higher particle number density than the average (Squires & Eaton 1991; Eaton & Fessler 1994; Toschi & Bodenschatz 2009; Wood et al. 2005). If the chemical time scale is short compared to the life-time of the clusters, the reactant concentration within the clusters will be much lower than outside the clusters. On the other hand, if the particle number density is low, the particle clusters will not have enough time to consume a significant fraction of the reactant during the life-time of the cluster, and hence, the reactant concentration will be roughly the same inside as it is outside the clusters. By assuming that the life-time of the clusters is of the order of the turbulent time scale, it is clear that the reactant concentration of particle flows with low Damköhler number will behave as if the particles were homogeneously distributed over the volume, i.e.; for small Damköhler numbers there is no effect of particle clustering on the reactant consumption.

From Eqs. (2.16) - (2.19) it can be deduced that for the homogeneous case, and then also for all cases with low Damköhler numbers, the reactant consumption rate will scale linearly with the

Damköhler number for a given turbulent flow field, such that

$$\alpha_{\text{hom}} = \frac{\text{Da}}{\tau_L}\frac{\text{Sh}}{2}. \tag{2.20}$$

When relaxing the restriction to small Damköhler numbers, the effect of particle clustering eventually comes into play. Kruger et al. (2016) have shown that the reactant consumption rate is given by

$$\alpha = \frac{\alpha_c \alpha_{\text{hom}}}{\alpha_c + \alpha_{\text{hom}}} \tag{2.21}$$

when α_c is a cluster dependent decay rate. (Note that since Kruger et al. assumed the Sherwood number to be 2, their α_{hom} equals our $\alpha_{\text{Sh,Da}} = \text{Da}/\tau_L$.) From this expression, the following normalized reactant consumption rate is found

$$\tilde{\alpha}_{\text{Sh}} = \frac{\alpha_{\text{Sh}}}{\alpha_{\text{Sh,Da}}} = \frac{\alpha_c \tau_L}{\alpha_c \tau_L + \text{DaSh}/2}\frac{\text{Sh}}{2}. \tag{2.22}$$

when Sh is given by Eq. (1.3) and the corresponding relative velocity between the particle and the fluid is determined by a model (which will be obtained in the next subsection). For diffusion controlled reactions, the modified reaction decay rate, as given by Eq. (2.22), is a measure of the relative modification to the mass transfer rate due to the effect of turbulence. This means that a modified Sherwood number can now be defined that accounts for the effect of turbulence;

$$\text{Sh}_{\text{mod}} = 2\tilde{\alpha}. \tag{2.23}$$

In the limit of small Damköhler numbers, this expression reduces to $\text{Sh}_{\text{mod}} = \text{Sh}$, as expected.

By employing the modified Sherwood number given by Eq. (2.23), one can now use the common expression for the reactant consumption rate, as given by Eq. (2.16), to find the real reactant consumption rate. In most cases, however, one needs the particle conversion rate $\dot{n}_{\text{reac}}$ for individual particles, which is closely connected to the reactant decay rate. For diffusion controlled mass transfer, the particle conversion rate is given by $\dot{n}_{\text{reac}} = -\kappa X_\infty C_g$, where C_g is the molar concentration of the gas phase and the mass transfer coefficient is now found by using the modified Sherwood number (as given by Eq. (2.23)) in; Eq. (1.1)

$$\kappa = \frac{D\text{Sh}_{\text{mod}}}{d_p}. \tag{2.24}$$

In many applications, the mass transfer rate is not purely diffusion controlled. This can be accounted for by including the effect of reaction kinetics at the particle surface. The corresponding particle conversion rate can then be expressed as (Kruger et al. 2016)

$$\dot{n}_{\text{reac}} = -\frac{\lambda\kappa}{\lambda + \kappa} X_\infty C_g, \tag{2.25}$$

where λ is the surface specific molar conversion rate. Since the reaction kinetics is only dependent on the conditions at the particle surface, the surface specific molar conversion rate is not affected by the turbulence. This is, as we have already seen, not the case for the mass transfer coefficient, which is now given by Eq. (2.24). In this way, all the common machinery for calculating particle reaction rates can still be used since the effects of the turbulence are incorporated into the modified Sherwood number.

3. Results

In all of the following, statistically stationary homogeneous and isotropic turbulence is considered. The Reynolds number is varied by changing the domain size while maintaining constant

TABLE 1. Summary of the simulations. The fluid density is unity while the Schmidt number is 0.2 and the viscosity is 2×10^{-4} m^2/s for all the simulations. For every simulation listed here, a range of identical simulations with different Damköhler numbers have been performed.

Label	L (m)	N_{grid}	d_p	ρ_p	Re	Sh	St	τ_L	α_c	$\alpha_c \tau_L S t/S h$
1A	$\pi/2$	64^3	3.4×10^{-3}	50	80	2.5	1.0	1.6	0.9	0.63
2A	2π	128^3	19×10^{-3}	50	400	2.8	1.0	5	0.23	0.43
3A	8π	256^3	11×10^{-3}	500	2200	2.8	1.0	15	0.07	0.41
2AB	2π	128^3	19×10^{-3}	25	400	2.7	0.5	5	0.26	0.25
3AB	8π	256^3	11×10^{-3}	250	2200	2.6	0.5	15	0.09	0.26
2B	2π	128^3	11×10^{-3}	50	400	2.5	0.3	5	0.21	0.13
3B	8π	256^3	11×10^{-3}	150	2200	2.6	0.3	15	0.09	0.18
2C	2π	128^3	19×10^{-3}	5	400	2.4	0.1	5	0.55	0.12
3C	8π	256^3	11×10^{-3}	50	2200	2.4	0.1	15	0.20	0.13
2D	2π	128^3	19×10^{-3}	1.5	400	2.3	0.03	5	1.20	0.08
3D	8π	256^3	11×10^{-3}	16	2200	2.3	0.03	15	0.45	0.10
2E	2π	128^3	19×10^{-3}	0.5	400	2.2	0.001	5	4.10	0.10

viscosity and turbulent intensity. The Damköhler number is varied by changing the number density of particles, while keeping everything else the same. All relevant simulations are listed in table 1.

3.1. *The mean relative particle velocity*

In order to predict a representative value of the particle Sherwood number from Eq. (1.3), the particle Reynolds number Re_p is required. From Eq. (2.11) it is clear that this also requires the relative particle velocity u_{rel}, which will be found in this subsection.

Given a particle with a response time that equals the Stokes time;

$$\tau_p = \frac{S d_p^2}{18\nu}, \tag{3.1}$$

such that $\tau_k < \tau_p < \tau_L$, where τ_k is the Kolmogorov time scale and τ_L is the integral time scale. With respect to the particle-turbulence interactions, the turbulent power spectrum may be divided into three distinct regimes, based on the relation between the particle response time and the turbulent eddy turnover time τ_{eddy}. The first regime is defined as the section of the turbulent power spectrum where the turbulent eddies have turnover times that are much larger than the response time of the particles, i.e. where $\tau_{\text{eddy}} \gg \tau_p$. All the turbulent eddies in this regime will see the particles as passive tracers, which follow the fluid perfectly. I.e., there will be no relative velocity between the particles and the eddies. The third regime is defined as the part of the power spectrum where the turbulent eddies have much shorter time scales than the particles, i.e. where $\tau_{\text{eddy}} \ll \tau_p$. The eddies in regime three will see the particles as heavy bullets that move in straight lines, without being affected by the motion of the eddies. Hence, the velocity of these eddies will contribute to the relative particle-fluid velocity. The second regime is now defined as the relatively thin band in-between regimes one and three, where $\tau_{\text{eddy}} \approx \tau_p$. These are the eddies that are responsible for particle clustering, since they are able to accelerate the particles

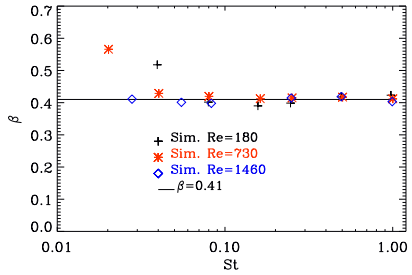

FIGURE 1. The parameter β, relating the relative particle velocity to the subscale velocity as defined in Eq. (3.9), is shown as a function of Stokes number.

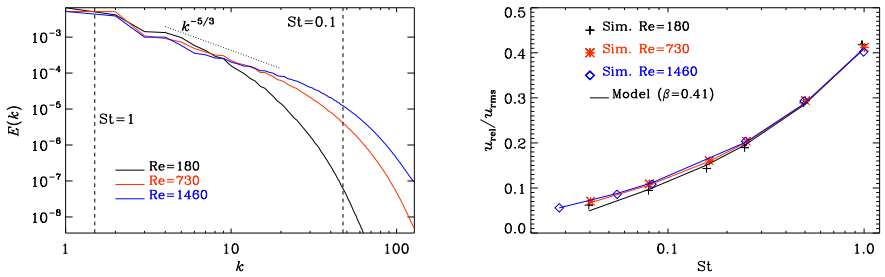

FIGURE 2. Left panel: kinetic energy spectrum for different Reynolds numbers. Right panel: relative particle velocity as a function of Stokes number.

to a level where they are thrown out of the eddy due to their inertia. In the following, we will refer to a typical eddy in regime two as a *resonant eddy*, and we define the scale of this eddy as ℓ. The resonant eddies are identified by their time scale, τ_ℓ, which is of the order of the particle response time, τ_p. For convenience, we set the two time scales equal, such that

$$\tau_\ell = \tau_p. \tag{3.2}$$

Based on the definitions above, it is clear that the largest turbulent eddies that yield a relative velocity between the fluid and the particles, are the resonant eddies. By assuming Kolmogorov scaling, the velocity of the resonant eddies is known to be $u_\ell = u_{\rm rms}(\ell/L)^{1/3}$, which can be combined with the above expression for the time scales to yield

$$k_\ell = k_L {\rm St}^{-3/2} \tag{3.3}$$

when the particle Stokes number is defined as

$${\rm St} = \frac{\tau_p}{\tau_L} \tag{3.4}$$

and $k_\ell = 2\pi/l$ and $k_L = 2\pi/L$ are the wave-numbers of the resonant eddies and the integral scale, respectively. In obtaining Eq. (3.3), it has also been used that the turnover time of the resonant eddies is $\tau_\ell = l/u_\ell$, while that of the integral scale eddies is $\tau_L = L/u_{\rm rms}$.

Since all scales smaller than ℓ will induce a relative velocity between the particles and the fluid, it is reasonable to assume that the relative velocity between the fluid and the particles will be a certain fraction β of the integrated turbulent velocity $\tilde{u}_\ell$ of all scales smaller than ℓ, such that

$$u_{\rm rel} = \beta \tilde{u}_\ell \tag{3.5}$$

when $\tilde{u}_\ell$ is defined as

$$\frac{1}{2}\tilde{u}_\ell^2 = \int_{k_\ell}^{k_\eta} E(k)dk \tag{3.6}$$

and $k_\eta = 2\pi/\eta$ is the wave-number of the Kolmogorov scale ($\eta = (\nu^3/\epsilon)^{1/4}$), where ϵ is the dissipation rate of turbulent kinetic energy. Integration of Eq. (3.6) yields

$$\tilde{u}_\ell = u_{\rm rms}\sqrt{\frac{k_\ell^{-2/3} - k_\eta^{-2/3}}{k_L^{-2/3} - k_\eta^{-2/3}}} \tag{3.7}$$

for $E(k) = c\epsilon^{2/3}k^{-5/3}$ when it has been used that the total turbulent kinetic energy is given by

$$\frac{1}{2}u_{\rm rms}^2 = \int_{k_1}^{k_\eta} E(k)dk, \tag{3.8}$$

where k_1 is the wavenumber of the largest scale in the simulation. Combining Eqs. (3.3) and (3.7) with Eq. (3.5) finally yields

$$u_{\rm rel} = \beta u_{\rm rms}\sqrt{\frac{{\rm St}k_L^{-2/3} - k_\eta^{-2/3}}{k_L^{-2/3} - k_\eta^{-2/3}}}. \tag{3.9}$$

The unknown constant in this equation, β, can be determined numerically from Eq. (3.5), i.e. $\beta = u_{\rm rel}/\tilde{u}_\ell$. Here, $u_{\rm rel}$ is found directly from DNS simulations, while $\tilde{u}_\ell$ is calculated from Eq. (3.7). It is seen from figure 1 that β is close to 0.41 for most Stokes and Reynolds numbers. The main exception is for low Reynolds and Stokes numbers, where β is significantly larger. This can be understood by inspecting the left panel of figure 2, where it is seen that for Re = 180 and St < 0.1, we are already far into the dissipative subrange, where our model is not expected to be correct since it relies on a Kolmogorov scaling.

It is surprising to see that Eq. (3.9) reproduces the relative particle velocity for such low Stokes numbers, even for the smaller Reynolds numbers. This may be explained by reconsidering Eq. (3.2), where we assumed that the resonant eddies correspond to the eddies that have *exactly* the same turnover time as the response time of the particles. This is just an order of magnitude estimate, and a more correct expression would probably be

$$\tau_\ell = \gamma\tau_p, \tag{3.10}$$

where γ is of the order of unity. More work should, however, be devoted to understanding the coupling between the particles and the turbulent eddies. In particular, a more exact definition of the resonant eddies is needed. We nevertheless believe that β is a universal property of the HIP approximation and the Navier-Stokes equations that will have a constant value for all Re and St as long as the resonant eddies are within the inertial range.

In the right panel of figure 2, the average relative particle velocity, as found from the DNS simulations (symbols), is compared with the predicted values from Eq. (3.9) (solid lines). It is seen that the fit is rather good for most Reynolds and Stokes numbers. This supports the use of Eq. (3.9) for predicting the relative particle velocity.

3.2. *The cluster size*

The typical size of the clusters ℓ is assumed to be the size of the resonant eddies. From Eq. (3.3) this yields a cluster size of

$$l = L{\rm St}^{3/2}. \tag{3.11}$$

It can be seen from figure 3 that the particle number density distribution does indeed show more small scale variation for the smaller Stokes numbers. This has been quantified in figure 4 where

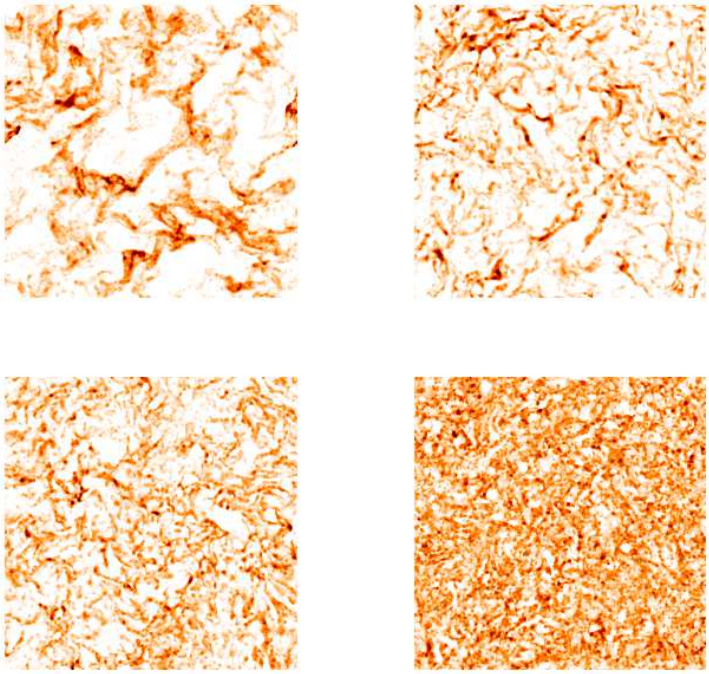

FIGURE 3. Particle number density for St = 1 (upper left), St = 0.3 (upper right), St = 0.1 (lower left) and St = 0.03 (lower right) (runs 3A, 3B, 3C and 3D in table 1).

the power spectrum of the particle number density is shown. Here we see that the spectrum peaks at large scales for St = 1 while the peak is located at much smaller scales for smaller Stokes numbers. The peak in the spectrum does not, however, follow Eq. (3.11) as accurately as expected. The reason for this is most likely that power spectra are not the right diagnostics to study the size of particle clusters, but it may also be partly because of: 1) poor statistics due to too few particles (the smaller clusters are not filled with particles), 2) the constant in the definition of the resonant eddies not being unity (see e.g. Eq. (3.10)), or 3) finite Reynolds number effects.

The power spectrum P can be integrated to yield a measure of the strength in the particle number density fluctuations, given by the root-mean-square (rms) particle number density;

$$n_{\text{rms}} = \int P dk. \tag{3.12}$$

It is found that the rms particle number density is decreasing with Stokes number. More specifically, n_{rms} is 1.6, 1.5, 1.2 and 0.8 for Stokes numbers of 1, 0.3, 0.1 and 0.03, respectively. This means that the high density regimes have higher particle number densities for larger Stokes numbers.

3.3. *Reactant consumption rate*

The normalized reactant consumption rate is shown in figure 5. The symbols correspond to the results from the DNS simulations, while the solid lines are given by Eq. (2.22). Here, the Stokes number is found by using the model for the relative velocity, as given by Eq. (3.9), in the expression for the Sherwood number (Eq. (1.3)). The value of the cluster decay rate, α_c, is the only free parameter and it is chosen by a best fit approach. The values of α_c are found in table 1.

The value of $\tilde{\alpha}$ for small Damköhler numbers equals the Sherwood number divided by two,

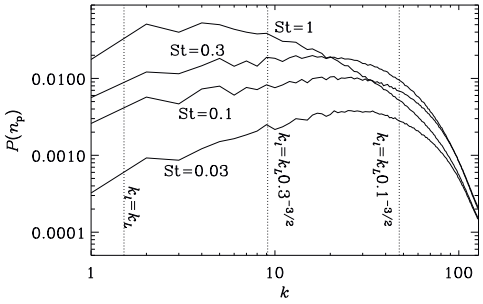

FIGURE 4. Power spectrum of particle number density for runs 3A, 3B, 3C and 3D in table 1.

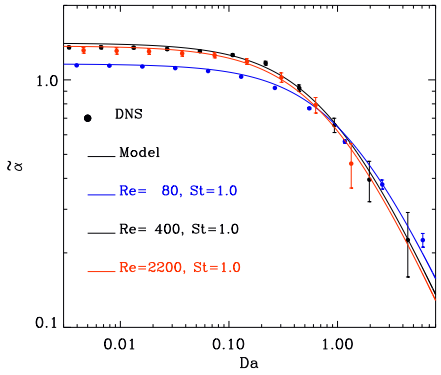

FIGURE 5. Normalized decay rate as a function of Damköhler number for Stokes number of unity (runs 1A-3A).

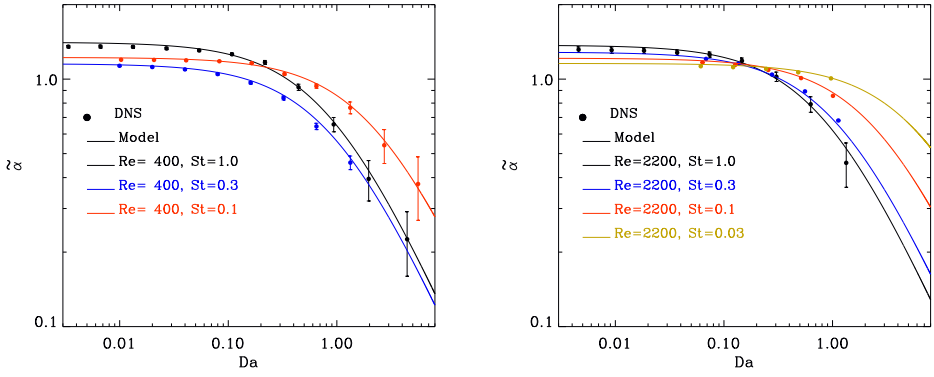

FIGURE 6. Normalized decay rate as a function of Damköhler number for different Stokes numbers. The left panel show the results for Re = 400 (runs 2A-C) while the right panel is for Re = 2200 (runs 3A-3D).

while the Damköhler number for which $\tilde{\alpha}$ starts to decrease is determined by the cluster decay rate α_c. Overall, the model seems to follow the results from the DNS simulations rather well.

From figure 5 it can be seen that for large Stokes numbers, the curves for the normalized decay rates of a given Stokes number overlap for different Reynolds numbers if the Reynolds number is high enough. This is because the resonant eddies are at scales larger than the dissipative subrange.

So increasing the Reynolds number, which may be considered a shift of the dissipative subrange to smaller scales, is not affecting the resonant eddies, and hence also the clustering is unaffected. If, however, the Reynolds or the Stokes number is small, such that the resonant eddies are in the dissipative subrange, a change in Reynolds number will have an effect on the normalized decay rate ($\tilde{\alpha}$).

Figure 6 shows that by decreasing the Stokes number, the normalized reactant decay rate stays unchanged up to larger Damköhler numbers. This means that the effect of particle clustering is weaker for smaller Stokes numbers. This is expected since the limit of very small clusters corresponds to individual particles, where $\tilde{\alpha}$ is independent of Da. From the simulations with small Damköhler numbers and Re = 2200, which are shown in the right panel of figure 6, it can be observed that the normalized decay rate is monotonically decreasing with Stokes number. The reason for this is that for these simulations the particle size is kept constant as the Stokes number is changed, such that the Sherwood number is decreased with decreasing Stokes number. This is, however, not the case for the simulations with Re = 400, where it is found that the normalized decay rate for small Damköhler numbers is lower for St = 0.3 than for St = 0.1. The reason for this is that a smaller particle radius was used for the simulations with St = 0.3. The effect of reducing the particle radius is that the particle Reynolds number, and hence also the Sherwood number, is decreased.

3.4. *The cluster decay rate*

If the chemical time scale is much shorter than the lifetime of the particle clusters, the interior of the clusters will quickly be void of reactants. This means that the reactant consumption rate is controlled by the flux of reactant to the surface of the clusters, where the reactant will be consumed at the exterior of the cluster. Based on this, it is clear that for large Da (small τ_c), the clusters behave as large solid particles, or super-particles. Following Kruger et al. (2016), the reactant decay rate is then given by the so called cluster decay rate;

$$\alpha_c = n_c \kappa_c A_c \tag{3.13}$$

when $n_c = A_1 l^{-3}$ is the number density of clusters (or super-particles), $\kappa_c = D_t \mathrm{Sh}/l$ is the reactant diffusion rate to the super-particles, $A_c = A_2 l^2$ is the surface area of the clusters, D_t is the turbulent diffusivity that carries the reactant from the surrounding fluid to the surface of the clusters and A_1 and A_2 are constants that depend on the dimensionality of the clusters. It is clear that turbulent eddies larger than ℓ, as given by Eq. (3.11), can not participate in the turbulent transport of reactants to the clusters, while eddies slightly smaller than ℓ will participate. A first approximation of the turbulent diffusivity to the surface of the clusters is therefore given by

$$D_t = u_\ell l = u_L L \mathrm{St}^2. \tag{3.14}$$

By combining the above, taking into account Eq. (3.11), it can be found that

$$\frac{\alpha_c \tau_L \mathrm{St}}{\mathrm{Sh}} = A_1 A_2, \tag{3.15}$$

where the right hand side should be constant for resonant eddies well inside the inertial range. From figure 7, it can be seen that the right hand side of the above equation is constant only for Stokes numbers smaller than ~ 0.3. Since the value of the right hand side starts to increase already for St = 0.3, this may once again indicate that γ from Eq. (3.10) is different from unity. The discrepancy may also be due to the fact that when it comes to the shape of the particle clusters, a large scale strain may stretch the particle clusters. For St $\sim$ 1, there are no vortices that are larger than the clusters, and hence the dimensionality of the clusters becomes different. This will inevitably yield different values of $A_1 A_2$. The value of the geometric coefficients can be

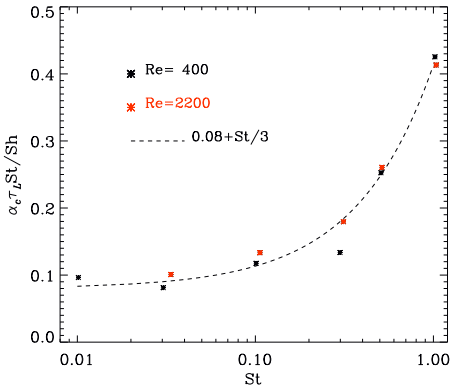

FIGURE 7. The product $\alpha_c \tau_L \mathrm{St}$ as a function of St for runs with resonant eddies in the inertial range.

fitted by

$$A_1 A_2 = 0.08 + \mathrm{St}/3, \tag{3.16}$$

but this is just an empirical fit and more work is required in order to understand the fundamentals behind the shape and size of the particle clusters.

4. Conclusion

In this work, the effect of turbulence on the mass (and heat) transfer between inertial particles and the embedding fluid is studied. The turbulence is shown to have two effects on the mass transfer. The first effect is active for all Damköhler numbers, and here the turbulence increases the mass transfer rate due to the relative velocity between the particles in the fluid. A corresponding model for the relative velocity between the fluid and the particles is given by Eq. (3.9) which uses basic variables of the flow. With this, adding effects of relative velocity into RANS based simulations is possible.

The second effect with which turbulence influences the mass transfer rate is through the clustering of particles. It is shown that the size of the particle clusters increases with the particle Stokes number, and that the clustering decreases the overall mass transfer rate between the particles and the fluid. This is a confirmation of the findings of Kruger et al. (2016). In addition, a model is developed that takes this effect into account and incorporates it into a modified Sherwood number. This model is shown to give reasonable results for Stokes numbers (based on the turbulent integral scale) less than ~ 0.3, while an empirical fit is employed to account for Stokes numbers up to unity. More work is still required in order to fully understand the size and dimensionality of the the particle clusters. As of now, a unique way of characterizing particle clusters does not exist, and very little work has actually been put into the study of large-scale clustering of particles.

Acknowledgements

The research leading to these results has received funding from the Polish-Norwegian Research Program operated by the National Centre for Research and Development under the Norwegian Financial Mechanism 2009-2014 in the frame of Project Contract No Pol-Nor/232738/101/2014. This work was supported by the grant "Bottlenecks for particle growth in turbulent aerosols from the Knut and Alice Wallenberg Foundation, Dnr. KAW 2014.0048 and by grant from Swedish

Research Council (Dnr. 638-2013-9243). NELH and DM also acknowledge the Research Council of Norway under the FRINATEK grant 231444.

REFERENCES

W. P. Jones and B. E. Launder, Int. J. Heat Mass Transfer **15**, 301 (1972).
S. B. Pope, *Turbulent flows*. Cambridge University Press (2003).
L. Schiller and A. Naumann, Ver. Deut. Ing **77**, 318 (1933).
C. T. Crowe, *Multiphase Flows Droplets*. CRC Press (2012).
B. F. Magnussen and B. H. Hjertager, 16'th Symposium (International) on Combustion, pp. 719-729. Pittsburgh: The Combustion Institute (1976).
I. S. Ertesvåg and B. F. Magnussen , Combust. Sci. Technol. **159**, 213 (2000).
C. Dopazo, (ed. P. A. Libby and F. A. Williams), pp. 375-474. London: Academic Press. (1994).
W. E. Ranz and W. R. Marshall, Chem Engr. Prog. **48**, pps. 141 and 173 (1952).
J. Kruger, N. E. L. Haugen, T. Lovas and D. Mitra *Proc. Comb. Symp.*, dx.doi.org/10.1016/j.proci.2016.06.187
A. Silaen and T. Wang, Int. J. Heat Mass Transfer **53**, 2074-2091 (2010).
M. Vascellari, S. Schulze, P. Nikrityuk, D. Safronov and C. Hasse, Flow turbulence and combustion **92**, 319-345 (2014).
M. Vascellari, D. G. Roberts, S. S. Hla, D. J. Harris and C. Hasse, Fuel **152**, 58-73 (2015).
A. Klimanek, W. Adamczyk, A. Katelbach-Wozniak, G. Wecel and A. Szlek, Fuel **152**, 131-137 (2015).
L. Chen, S. Z. Yong and A. F. Ghoniem, Progress in energy and combustion science **38**, 156-214 (2012).
C. Chen, M. Horio and T. Kojima, Chemical Engineering Science **55**, 3875-3883 (2000).
J. Gao, C. Xu. S. Lin and G. Yang, AIChE Journal **45**, 1095-1113 (2004).
Y. Zhang, X.-L. Wei, L.-X. Zhou and H.-Z. Sheng, Fuel **84**, 1798-1804 (2005).
K. Luo, H. Wang, J. Fan and F. Yi, Energy and Fuels **26**, 6128-6136 (2012).
T. Brosh and N. Chakraborty, Energy and Fuels **28**, 6077-0688 (2014).
T. Brosh, D. Patel, D. Wacks and N. Chakraborty, Fuel **145**, 50-62 (2015).
T. Hara, M. Muto, T. Kitano, R. Kurose and S. Komori, Combustion and Flame **162**, 4391-4407 (2015).
N. G. Deen and J. A. M. Kuipers, Chemical Engineering Science **116**, 645-656 (2014).
A. Johansen, J. S. Oishi, M.M.Mac Low, H. Klahr, T. Henning, and A. Youdin, Nature **448**, 1022 (2007).
N. E. L. Haugen and S. Kragset, J. Fluid Mech. **661**, 239 (2010).
N. E. L. Haugen, N. Kleeoring, I. Rogachevskii and A. Brandenburg, Phys. Fluids **24**, 075106 (2012).
The Pencil-Code, http://pencil-code.nordita.org/
N. E. L. Haugen and A. Brandenburg, Phys. Fluids **18**, 075106 (2006).
E. Calzavarini, M. Kerscher, D. Lohse and F. Toschi, J. Fluid Mech. **607**, 13-24 (2008).
M. M. Baum and P. J. Street, Combustion Science and Technology **3**, 231-243 (1971).
J. Bec, L. Biferale, M. Cencini, A. Lanotte, S. Musacchio and F. Toschi, Physical Review Letter **98**, 084502 (2007).
K. D. Squires and J. K. Eaton, Journal of Fluid Mechanics **226**, 1-35 (1991).
A. M. Wood, W. Hwang and J. K. Eaton, International Journal of Multiphase Flow **31**, 1220-1230 (2005).
J. K. Eaton and J. R. Fessler, International Journal of Multiphase Flow **20**, 169-209 (1994).
F. Toschi and E. Bodenschatz, Annual Review of Fluid Mechanics **41**, 375-404 (2009).